



Supplement of

Development of a cascade impactor optimized for size-fractionated analysis of aerosol metal content by total reflection X-ray fluorescence spectroscopy (TXRF)

Claudio Crazzolara and Andreas Held

Correspondence to: Claudio Crazzolara (crazzolara@tu-berlin.de)

The copyright of individual parts of the supplement might differ from the article licence.

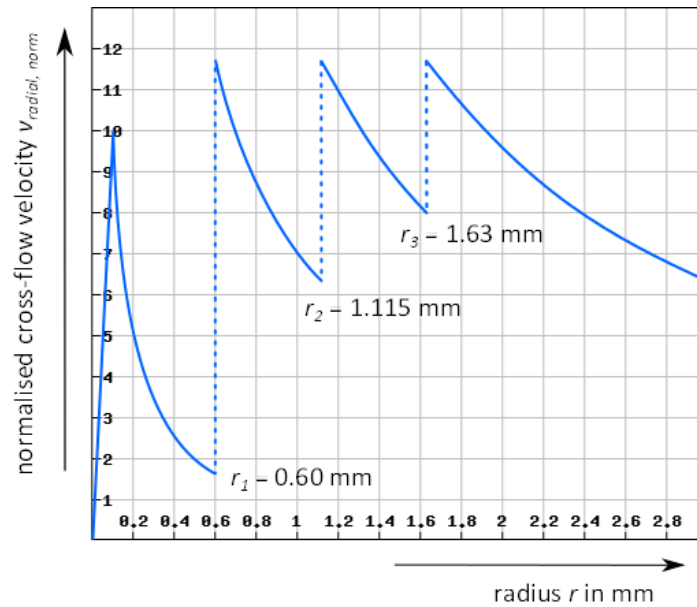


Figure S1. Mean normalized radial crossflow velocity $v_{\text{radial, norm}}$ as a function of radius r . The average velocity of the radial cross flow v_{radial} is a function of the radius r starting from the centric nozzle at $r = 0$ and decreasing with a $1/r$ characteristic. When r approaches the value of the radius r_1 of the first nozzle circle the velocity v_{radial} increases rapidly to a local maximum due to the air inflow through the nozzles of the first nozzle circle. With further increasing radius r , the mean velocity of the radial crossflow v_{radial} decreases again with a $1/r$ characteristic until the value of the radius r_2 of the second nozzle circle is reached, where v_{radial} increases to the next local maximum. The velocity is normalised to the value of the maximum of the velocity of the radial cross flow at the edge of the centric nozzle ($r = 0.1$ mm).

Table S1. Comparison of nominal and measured nozzle diameters of impactor stages 1 to 5

Stage	Number of nozzle(s)	Nominal diameter of nozzle(s)	Mean value of measured diameter(s) of nozzle(s)	Absolute difference of the mean value between measured and nominal diameter	Relative difference of the mean value between measured and nominal diameter	Absolute standard deviation of all nozzles of a stage	Relative standard deviation
	N	d_n	$d_{n,m}$	$d_{n,m} - d_n$	$(d_{n,m} - d_n) / d_n$	<i>stdev</i>	<i>stdev</i> / $d_{n,m}$
1	1	6.500 mm	6.641 mm	+0.141 mm	+2.2 %		
2	1	2.600 mm	2.610 mm	+0.010 mm	+ 0.4 %		
3	7	0.750 mm	0.749 mm	-0.001 mm	-0.1 %	0.0020 mm	0.3 %
4	19	0.200 mm	0.204 mm	+ 0,004 mm	+2.0 %	0.0004 mm	0.2 %
5	24	0.200 mm	0.203 mm	+ 0,003 mm	+1.5 %	0.0023 mm	1.1 %

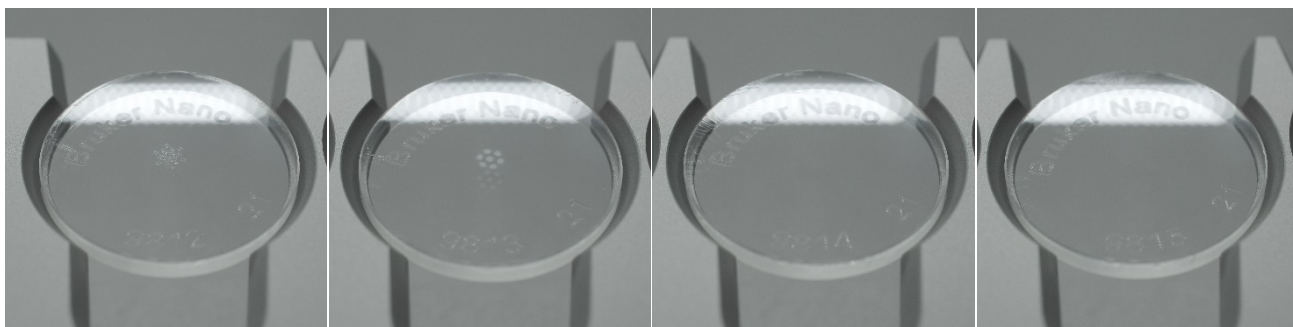


Figure S2. Four photographs with perspective views of four sample carriers at the following stages: From left to right, sample carriers no. 9812 and no. 9813 are shown after operating for 30 minutes at 5 slm with particle-laden atmospheric air in stages 4 and 3. In accordance with the results of TXRF analysis no. 7, particle deposits are clearly visible in the centre of both sample carriers as the result of sampling a total of 150 volumetric litres of atmospheric air at standard conditions (293 K, 1013 hPa). For sample carrier No. 9812, the particle deposits reflect the arrangement and number of a total of 19 nozzles (one in the centre, six each on three concentric circles) of impactor stage 4, whereas for sample carrier no. 9813, the particle deposits reflect the arrangement and number of a total of 7 nozzles (one in the centre, six on one circle) of impactor stage 3. Sample carriers no. 9814 and no. 9815 in the right half are shown after operating for 15 minutes at 5 slm with particle-free air in the “potentially particle contaminated” impactor in stages 4 and 3 corresponding to TXRF analysis no. 9. No particle deposits are visible on these two sample carriers.

Table S2. Results of three consecutive particle collection periods on 29 August 2022 at Potsdamer Platz, Berlin, Germany. The mass concentrations of various elements (in ng m⁻³) in the particle fractions PM 10, PM 2.5 and PM 1 are shown.

	Sampling period 1 (8:00 till 8:30 CEST)			Sampling period 2 (8:32 till 9:02 CEST)			Sampling period 3 (9:06 till 9:36 CEST)		
	mass concentration in ng m ⁻³			mass concentration in ng m ⁻³			mass concentration in ng m ⁻³		
	PM10	PM2.5	PM1	PM10	PM2.5	PM1	PM10	PM2.5	PM1
Fe	811	326	70	379	338	72	733	274	56
Zn	22.5	13.9	5.8	21.1	20.2	8.1	31.8	18.4	8.5
Cu	30.4	13.5	2.7	12.6	11.4	2.3	22.9	9.4	2.1
Mn	8.0	3.2	0.9	4.2	3.7	1.4	9.3	4.1	1.8
Pb	1.1	0.9	0.6	1.6	1.5	0.9	1.7	1.1	0.8
Ni	0.6	0.3	0.2	0.4	0.3	0.1	0.6	0.3	0.2